

Article

In Situ Generation of Hydrogen Peroxide Using Polymetallic-Doped g-C₃N₄ for Pollutant Removal

Liyan Wang^{1,2}, Jianqing Ma^{1,3,*}, Qianhui Guo¹, Liang Liu⁴, Jiangnan Shou¹, Aojie Sun¹ and Liaoyuan Zhao⁴

¹ School of Civil Engineering and Architecture, NingboTech University, Ningbo 315100, China; cpgzwly@163.com (L.W.); guoqh@nbt.edu.cn (Q.G.); shoujn@nbt.edu.cn (J.S.); 3190621168@nbt.edu.cn (A.S.)

² Polytechnic Institute of Technology, Zhejiang University, Hangzhou 310015, China

³ Ningbo Research Institute, Zhejiang University, Ningbo 315100, China

⁴ Blue City Ecological Co., Ltd., Ningbo 315100, China; liuliang@bluecityeco.com (L.L.); zhaoly@bluecityeco.com (L.Z.)

* Correspondence: majq@nit.zju.edu.cn; Tel./Fax: +86-18367463842

Abstract: Fenton reaction is a powerful technology for pollutants' removal from water. However, the cost of H₂O₂ becomes one of the major stumbling blocks in its application. H₂O₂ has a relatively high price and is easily decomposed during transportation and use; therefore, in situ synthesis of H₂O₂ could improve economic benefits effectively. In this study, a Fe/Ni/Pd ternary metal-doped graphitic carbon nitride (FeNi-Pd@CN) is prepared, and in situ H₂O₂ generation using formic acid as hydrogen sources for organics removal was proved. The catalyst is advantageous, as H₂O₂ could accumulate to 1.69 mmol/L in 150 min when pumping air rather than oxygen gases in other studies. Furthermore, 92.0% of Acid Red 73 (200 mg/L) and 93.2% of tetracycline hydrochloride (10 mg/L) could be removed in 150 min without any pH adjustment. Characterization results show that the catalyst has good stability in metal leaching and reuse tests. It is proved that •OH and •O₂⁻ are the main reactive oxygen species, and a synergistic effect between Fe and Ni exists that enhances ROS generation for organics degradation. This work offers a promising method to remove refractory organic contaminants from industrial wastewater.

Keywords: in situ generation; hydrogen peroxide; pollutant removal; graphitic carbon nitride



Citation: Wang, L.; Ma, J.; Guo, Q.; Liu, L.; Shou, J.; Sun, A.; Zhao, L. In Situ Generation of Hydrogen Peroxide Using Polymetallic-Doped g-C₃N₄ for Pollutant Removal. *Appl. Sci.* **2021**, *11*, 10797. <https://doi.org/10.3390/app112210797>

Academic Editors: Petr Korusenko and Sergey Nesov

Received: 19 October 2021

Accepted: 9 November 2021

Published: 15 November 2021

Publisher's Note: MDPI stays neutral with regard to jurisdictional claims in published maps and institutional affiliations.



Copyright: © 2021 by the authors. Licensee MDPI, Basel, Switzerland. This article is an open access article distributed under the terms and conditions of the Creative Commons Attribution (CC BY) license (<https://creativecommons.org/licenses/by/4.0/>).

1. Introduction

Refractory organic contaminants in industrial wastewater are often intractable to the traditional wastewater system and harmful to the environment, thus their treatment technologies have attracted extensive attention worldwide. Fenton reaction is viewed as a useful and feasible method to remove these pollutants [1]. It involves the transformation of H₂O₂ into strongly oxidized hydroxyl radicals (•OH) under the catalyzation of Fe²⁺, which could subsequently promote radical chain reactions leading to the degradation of refractory organic compounds [2]. However, the application of Fenton reactions was limited to strict acidic conditions, and plentiful iron sludge would be formed during the reactions [3]. On the other hand, the cost of H₂O₂ is also one of the major stumbling blocks in its application. It seems that the heterogeneous Fenton-like technology with low H₂O₂ consumption could overcome these shortcomings and significantly improve the ability of water treatment [4].

As a green and efficient oxidant, the demand for hydrogen peroxide in many fields is increasing year by year [5–7]. H₂O₂ has active chemical properties and is difficult to preserve and transport. In a typical Fenton reaction, the addition amount of H₂O₂ should far exceed the stoichiometric ratio. That is, much H₂O₂ added was consumed ineffectively in reactions. For example, Li et al. [8] calculated that 25.4% of added H₂O₂ was utilized for organic degradation in a homogeneous system, while the efficiency is only 0.4% in a heterogeneous Fe₃O₄/H₂O₂ system. Excess H₂O₂ is prone to decompose to O₂ on the

catalyst surface. From this point of view, the slowly in situ generation of H_2O_2 and its direct transformation into ROS is a feasible method to prevent the waste of H_2O_2 .

The direct synthesis of hydrogen peroxide using hydrogen and oxygen as raw materials and noble metal as catalysts has attracted much attention [9,10]. In the field of wastewater treatment, it seems that formic acid is one of the most promising hydrogen carrier materials. Although the hydrogen content in formic acid is only 4.4 wt%, the hydrogen production performance is superior to that of most other hydrogen-containing materials in terms of simplicity, availability to net capacity ratio, and experimental environment [11,12]. More importantly, formic acid is biodegradable, and its acidity averts extra pH adjustment for Fenton-like reactions. It is particularly suitable for the pretreatment of industrial wastewater, which contains lots of refractory organic contaminants. Previous studies have reported the Pd-based catalysts for the successful generation of H_2O_2 using formic acid [13]; however, when used in organic removals, pure oxygen and pH adjustment are still in need [13]. To further simplify the process and lower the cost, a more active catalyst that could facilitate the formic acid dehydrogenation and $\bullet OH$ yielding is aimed to fabricate in this study.

Graphitic carbon nitride ($g-C_3N_4$) is a graphite-like material with stable chemical properties [14]. $g-C_3N_4$ can be synthesized by simple pyrolysis through low-cost N-rich precursors such as melamine, ammonium thiocyanate, urea, and thiourea [15]. Its popularity originates from the ability as a non-metal catalyst for H_2 yielding through water splitting. Later studies reveal its versatile properties in several fields, for example, Fenton-like reactions [16]. Basically, $g-C_3N_4$ could accelerate the catalytic ability in two ways: one is the anchor of metal atoms and the other is to increase the electron conduction rate as a transport carrier [17,18]. Therefore, the present study aims to design a Fe, Ni, Pd co-doped $g-C_3N_4$ composite with enhanced catalytic ability for organic removal. Through the complex with $g-C_3N_4$ and the synergistic effects of different metals, H_2O_2 could be produced easily after the rapid decomposition of formic acid. This system with simplicity in operation will propel the practical application of Fenton-like reactions for organic removal by the in situ H_2O_2 route.

2. Materials and Methods

2.1. Materials

Dicyandiamide (DCD, CP, 98%), $NiCl_2 \cdot 6H_2O$ (AR, 99%), $FeCl_3 \cdot 6H_2O$ (AR, 99%), and Formic acid aqueous solution (AR, 88%) were obtained from Sinopharm Chemical Reagent Co., Ltd. (Shanghai, China). H_2O_2 (GR, 30% w/w) was purchased from National Medicines Corporation Ltd. of Shanghai, China. $PdCl_2$ (AR, 59–60%) was purchased from Shanghai Macklin Biochemical Co., Ltd. (Shanghai, China). Tetracycline hydrochloride (TC) was obtained from Shanghai Aladdin Biochemical Technology Co., Ltd. (Shanghai, China). Acid Red 73 (AR 73) was purchased from Chengdu West Asia Chemical Reagent Co., Ltd. (Chengdu, China). The deionized water used throughout this study was provided by a UPK/UPT ultrapure water system.

2.2. Catalysts Preparation

Polymetallic-doped $g-C_3N_4$ ($M@CN$) catalysts were fabricated via a thermal process using dicyandiamide as a precursor. In a typical process, 2 g of dicyandiamide, 0.25 mM $FeCl_3 \cdot 6H_2O$, and 0.25 mM $NiCl_2 \cdot 6H_2O$ were dissolved in 20 mL water with continuous stirring and heating to form a clear solution. The resulting solution was dried in an oven at 70 °C until the entire excess moisture was evaporated. The dried catalyst precursor was calcined under a nitrogen atmosphere at 550 °C for 4 h. The as-obtained material was dispersed in $PdCl_2$ (7.5 mmol/L, 20 mL) solution and then ultrasonic treated for 15 min (the amount of Pd added in all samples in this paper remains unchanged). Subsequently, the resulting solution was slowly added to $NaBH_4$ aqueous solution with stirring. The samples were washed three times with distilled water and then dried in a vacuum drying chamber at 80 °C. The final product was labeled as FeNi-Pd@CN. For comparison, FeNi-

Pd@CN with different metal contents, Fe-Pd@CN, and Ni-Pd@CN were also prepared by the same method.

2.3. Characterization Methods

Characterization powder X-ray diffraction (XRD) for the crystal structure of the products was measured in an X'Pert PRO Multi-purpose X-ray Diffraction System (Bruker D8 advance, Karlsruhe, Germany) using Cu K radiation ($\lambda = 0.1541$ nm). Fourier transforms infrared (FTIR) spectra were obtained using a Nicolet 6700 FTIR Microscope spectrometer (Thermo Fisher, Waltham, MA, USA) to identify the functional groups. The X-ray photoelectron spectroscopy (XPS) data were recorded on an ESCALAB 250Xi X-ray photoelectron spectrometer (Thermo Fisher, Waltham, MA, USA). The scanning electron microscopy (SEM) was performed on a scanning electron microscope (SEM, FEI, Hillsboro, OR, USA). The high-resolution transmission electron microscopy (HRTEM) observations were carried out using a Tecnai G2 F30. High-resolution Transmission electron Microscope (HRTEM, FEI, Hillsboro, OR, USA) equipped with a high angle annular field (HADDF) detector. Nitrogen adsorption-desorption isotherm was determined by the JW-BK132F instrument (JWGB, Beijing, China).

2.4. Performances Tests

H₂O₂ synthesis and degradation activity were evaluated using a modified catalytic agent under ambient conditions. Specifically, 0.2 g of the catalyst and 2 mL of formic acid were added to 100 mL of AR-73 (200 mg/L) or TC (10 mg/L) solutions. At the same time, the suspension was stirred and blown with air (200 mL/min). Then, the suspension was stirred and sampled at regular intervals and filtered with 0.45 μ m filter membrane to determine the concentration of the solution.

TC was quantified using high-performance liquid chromatography (HPLC, Shimadzu LC-2030C 3D, Tokyo, Japan). The measurement condition of TC includes a C18 column, 0.1% formic acid and acetonitrile (71:19) mobile phase, 25 °C, and the corresponding detection wavelength is 356 nm. AR 73 was analyzed by UV/VIS spectrophotometer (Perkin Elmer Lambda 850, Waltham, MA, USA) at 509 nm. The H₂O₂ was measured using the titanium sulfate spectrophotometric method. The concentrations of leaching ions during the reaction were determined by inductively coupled plasma mass spectroscopy (ICP-MS, Perkin Elmer Nexion 300, Waltham, MA, USA).

3. Results and Discussion

3.1. Morphology and Structure

The morphology and structure of the as-synthesized FeNi-Pd@CN catalyst were firstly characterized by SEM and HRTEM images. It can be seen from Figure 1 that the particles with several micrometers were the stack of broken layers. The specific surface area (S_{BET}) of FeNi-Pd@CN was 9.18082 m²/g, calculated by the nitrogen adsorption-desorption isotherm. The isotherm curves were characteristic of a typical IV isotherm with an H3 hysteresis loop, indicating the slit-shaped pores formed by the plate-like particles aggregation (Figure S1). Palladium deposition on the surface of FeNi-Pd@CN could be observed in Figure 1b,c, as its crystalline interplanar spacing of 0.224 nm was assigned to Pd (111) plane [19]. Further exploration found that tiny particles with typical (104) planes of α -Fe₂O₃ were embedded in the carbon nitride matrix (Figure S2). Elements mapping also shows a small amount of aggregate Fe in Figure 1d,h. No obvious clusters related to Ni monocrystal species could be identified from HRTEM images, and Ni was evenly distributed in g-C₃N₄. The atomic contents of Fe, Ni, and Pd were 0.72, 0.91, and 0.03 at%, respectively (Table S1). Low content of Pd (0.27 wt%) ensured low prices for the catalyst preparation.

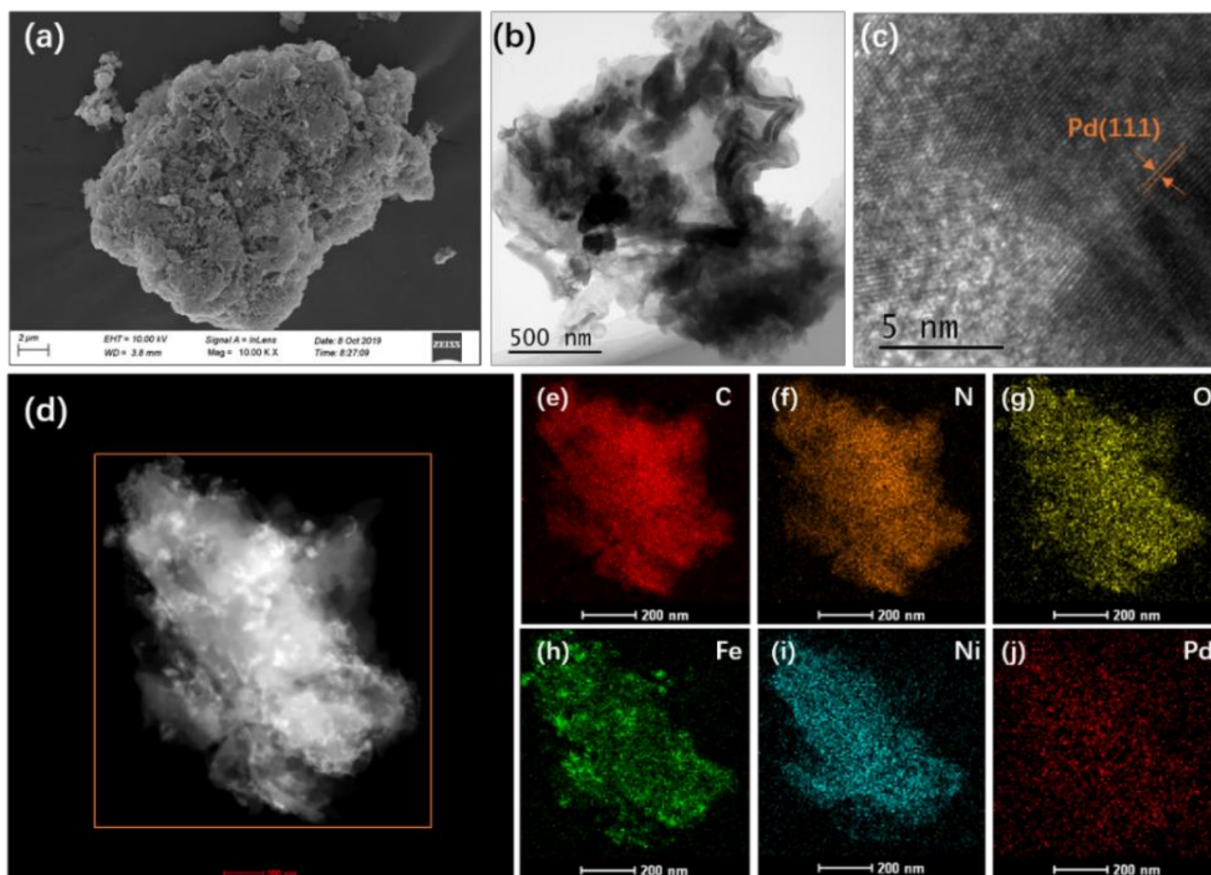


Figure 1. (a) SEM image of FeNi-Pd@CN; (b,c) HRTEM image of FeNi-Pd@CN; (d) HADDF images and (e–j) elemental mapping of FeNi-Pd@CN, C, N, O, Fe, Ni, and Pd.

3.2. Chemical Composition of the Catalyst

The chemical composition of the as-synthesized M@CN was examined by powder XRD, and the recorded patterns are presented in Figure 2a. Two peaks at 27.6 and 13.0 degrees were observed, which represented (002) and (100) facets of conjugated aromatic complexes, respectively [20]. After metal loading, the basic structure of g-C₃N₄ remained, but the graphitization degree of FeNi-Pd@CN was lower than two other M@CN. There are no obvious peaks related to metal crystal, perhaps due to the low content or small size of the metal species. These results were further confirmed by FT-IR spectra in Figure 2b. All three spectra show the characteristic peaks of g-C₃N₄: the peak at around 810 cm⁻¹ is attributed to the vibration of tris-*s*-triazine units [21], and the peaks in the region of 1100–1700 cm⁻¹ are attributed to the typical bands of aromatic C–N heterocycles containing either trigonal N(–C)₃ (full condensation) or bridging C–NH–C units (partial condensation), evidencing the formation of extended networks of C–N–C bonds [22]. The peaks between 3000 and 3600 cm⁻¹ are contributed by N–H stretching [21], and the much broader peaks of FeNi-Pd@CN verified that more free amino groups remained than Fe-Pd@CN and Ni-Pd@CN. The peak of FeNi-Pd@CN at 417.36 cm⁻¹ attributed to the stretching vibration of Fe–O [23] was also weaker than that of Fe-Pd@CN. It can be speculated that the addition of both Fe and Ni lower the graphitization degree, resulting in more defects in g-C₃N₄, and in the meantime, large aggregation of Fe species was avoided due to the combination of Fe precursor with amino groups. Previous literature [8] also pointed out the addition of Ni led to the small size and well-dispersed nanoparticles of Fe species.

The specific bonds and chemical states of FeNi-Pd@CN were further studied using X-ray photoelectron spectroscopy. The XPS survey spectrum (Figure 3a) of the M@CN composite displays the coexistence of C, N, O, Fe, Ni, and Pd elements. The C 1s region of

the spectra (Figure 3b) was fitted into three peaks. The main peak at 288.2 eV was assigned to sp^2 hybridized carbon corrected with N (C-N=C) [24], and two other peaks at 284.8 and 286.4 eV were typical signals of C-C and C-O components. Another $\pi-\pi^*$ satellite 6 eV from the main C1s peak could be observed, indicating the extended delocalized electrons structure of the g- C_3N_4 . The deconvolution of the N 1s XPS signals (Figure 3c) shows three major peaks at 398.9, 399.9, and 401.0 eV, which arise from sp^2 N atoms in triazine rings (C-N-C), sp^3 N atoms (HN-(C)₃), and the marginal amino(-NH₂), respectively [17,25]. The Ni 2p spectrum consists of a relatively narrow spin-orbit doublet (Figure 3d) characterized by binding energies of the Ni 2p_{3/2} and Ni 2p_{1/2} core levels of 855.7 and 873.4 eV, respectively [26–28], verifying the bipovalent nature of Ni. Fe 2p spectrum shows a mixture of core level and satellite features due to the existence of Fe²⁺ and Fe³⁺ [29]. Pd was partly reduced by NaBH₄; thus, its 3d spectrum displays two doublets caused by the Pd⁰ and Pd²⁺. The Pd 3d core level in this study (336.1 and 338.0 eV for 3d_{5/2} of Pd⁰ and Pd²⁺, respectively) shifted higher binding energy than values in NIST X-ray photoelectron spectroscopy database. This result manifests that Pd with small size supported on carbonaceous materials according to previous reports [30–32].

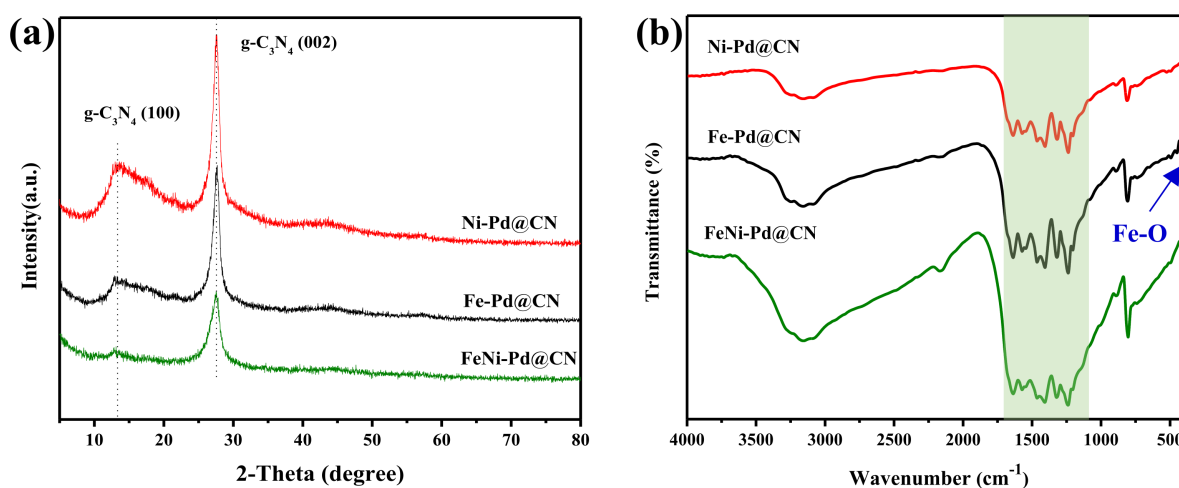


Figure 2. (a) XRD patterns of as-prepared catalysts and (b) FT-IR spectra of as-prepared catalysts, the green band reflects the typical stretching mode of tris-s-triazine in g- C_3N_4 .

3.3. The Catalytic Performances of Catalysts

The catalytic performance of the as-synthesized samples was firstly evaluated using a widely used azo dye, Acid Red 73 (AR 73). It can be seen from Figure 4a that the removal efficiency AR 73 (200 mg/L) catalyzed by FeNi-Pd@CN, Fe-Pd@CN, Ni-Pd@CN, and Pd@CN were 92.0%, 75.85%, 75.17%, and 41.06%, respectively. Clearly, the addition of Fe and Ni boosted the activity towards AR73 removal. Similar results were also found in the test of another common antibiotic, tetracycline hydrochloride (TC): 93.2% of TC (10 mg/L) was removed by FeNi-Pd@CN, which was higher than other metal-doped samples (Figure 4b). Fe and Ni could be the active sites for Fenton reactions, but as discussed in the previous part, their addition also lowers the graphitization degree of g- C_3N_4 , which means constantly adding metal does not always increase activity. Three excessive metal-doping samples (the addition of Fe: Ni were 2:1, 1:2, 2:2, respectively) were also prepared, and Figure S3 shows their TC removal efficiencies significantly reduced compared with FeNi-Pd@CN (the addition of Fe:Ni was 1:1).

The stability and recyclability of the FeNi-Pd@CN catalyst were evaluated by successive tests of AR 73 (Figure 5) degradation under the same reaction conditions. Only 6% of AR 73 removal efficiency decline was observed after four cycles, indicating good stability of the catalyst. XRD results in Figure S4 also show an almost unchanged spectrum after use. However, Due to the acidic environment caused by formic acid, metal leaching after the first cycle was

up to Fe 6.55 mg/L, Ni 4.93 mg/L and Pd 19.59 $\mu\text{g/L}$ measured by ICP-MS. It is speculated that either the unstable chemical bonds in the fresh catalyst samples are broken during the reaction or some metals are not fully anchored on the surface of $\text{g-C}_3\text{N}_4$. In the second cycle, the values decreased to acceptable values, with Fe 1.339 mg/L, Ni 711.068 $\mu\text{g/L}$ and Pd 6.767 $\mu\text{g/L}$, while there is almost no change in degradation activity. In practical applications, metal leaching problems during the first cycle could be solved in the later wastewater treatment procedures, or the catalyst could be pretreated by pickling before use.

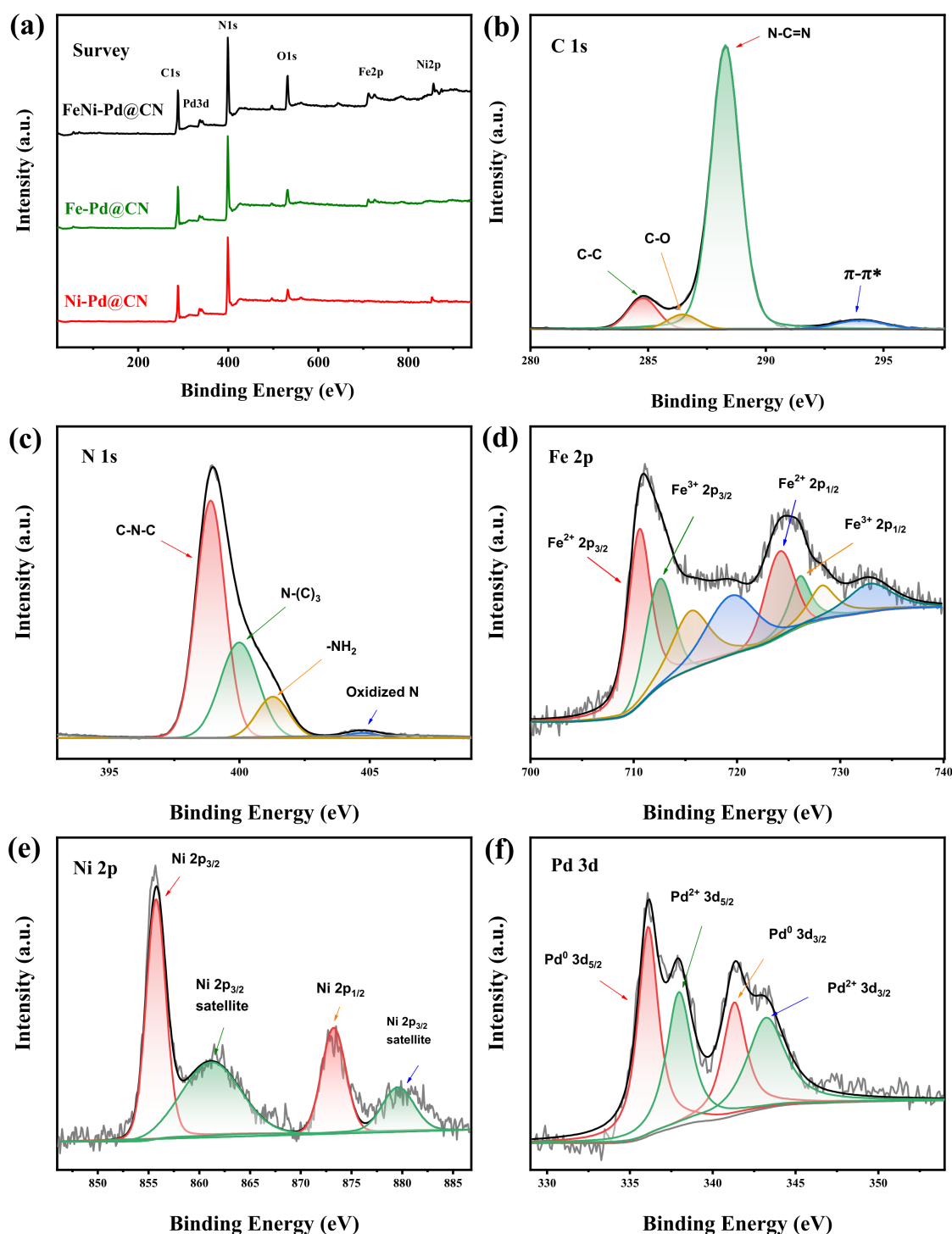


Figure 3. (a) XPS survey of samples. (b) C1s spectra; (c) N 1s spectra; (d) Fe 2p spectra; (e) Ni 2p spectra; and (f) Pd 3d spectra of FeNi-Pd@CN.

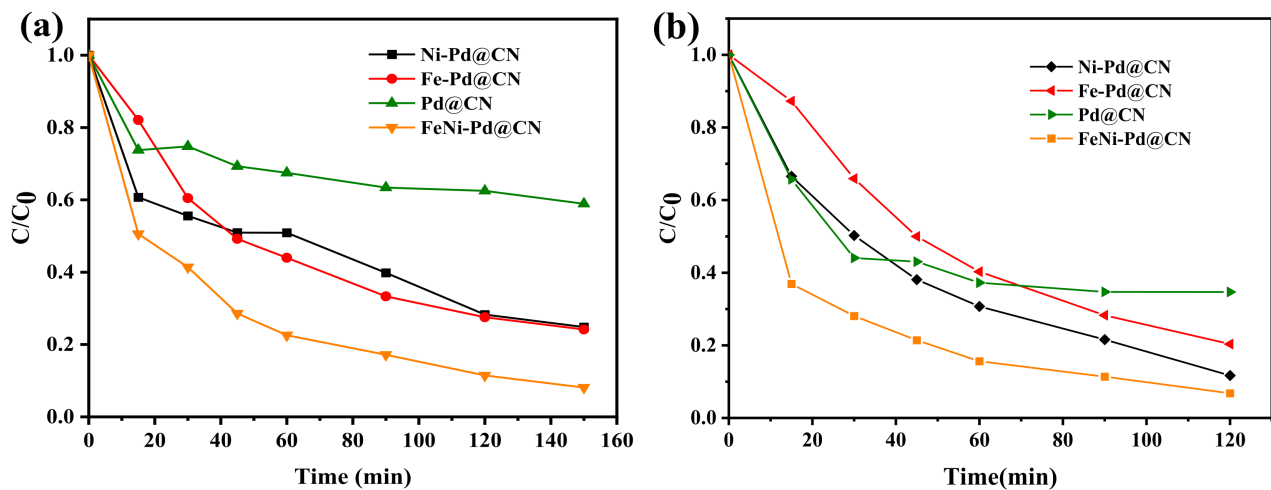


Figure 4. (a) Degradation of AR 73 (200 mg/L) and (b) TC (10 mg/L) by different catalysts (catalyst dosage: 2 g/L; FA: 46.6 mmol/L; air; 200 mL/min).

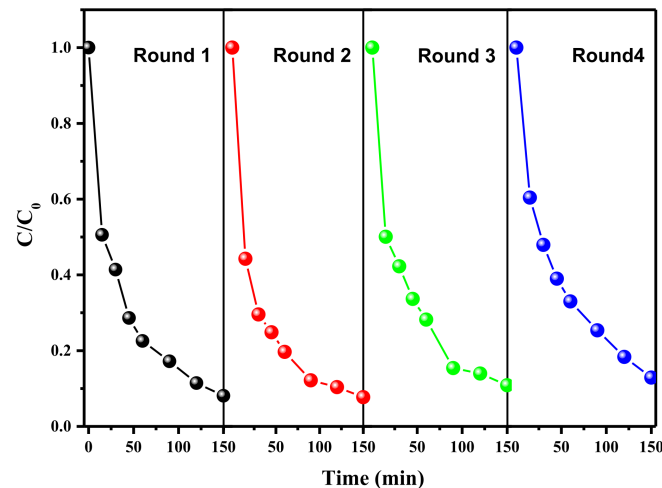


Figure 5. Degradation of AR 73 in multiple uses of FeNi-Pd@CN catalyst (AR 73 200 mg/L; catalyst dosage: 2 g/L; FA: 46.6 mmol/L; air; 200 mL/min).

3.4. Enhanced H₂O₂ Production

Direct generation of H₂O₂ from formic acid and O₂ using heterogeneous Pd was illustrated in previous reports. Basically, the process can be divided into two steps: first is the formic acid (FA) decomposition to H₂ (HCOOH → CO₂ + H₂), and second is O₂ reduction to H₂O₂ (H₂ + O₂ → H₂O₂). FA decomposition begins with the ionization of formic acid and then the cleavage of C-H bond in formate species as a vital step for H* forming (* denotes an active site). Qin et al. [33] summarized that strengthened adsorption of formate species and weakened adsorption of H* were favorable for hydrogen production through kinetic analysis. From these points of view, the addition of positively charged Fe and Ni is beneficial to the adsorption of HCOO* intermediates. However, the Pd 3d core level of FeNi-Pd@CN was almost similar to that of Fe-Pd@CN but higher than that of Ni-Pd@CN (Figure S5), suggesting that Fe is more capable than Ni of weakening the H* adsorption through the depletion of the d-band electronic state near the Fermi level [34].

In the second step, O₂ was firstly adsorbed and activated on Pd surface and then reduced to HOO* and H₂O₂* by adsorbed H atom. For high H₂O₂ selectivity and stability, the dissociation of O-O bond should be avoided. DFT results verified that Pd (111) has the lowest crystal surface energy compared to other facets and thus could reduce the dissociation of O-O bond in O₂*, HOO*, and H₂O₂* [35]. In this study, Pd supported on g-C₃N₄ exposes many crystal (111) facets and thus has high activity for H₂O₂ yielding.

An obvious accumulation of H_2O_2 could be observed even when blowing air by Pd@CN (Figure 6). According to experimental data as well as theory results [36], O_2 is easier to chemically adsorb on Fe and Ni ($\text{Fe} > \text{Ni} > \text{Pd}$); O_2 temperature-programmed desorption (O_2 -TPD) curves in Figure S6 also suggested that more adsorbed O and lattice O were introduced with the addition of Fe, and thus H_2O generation would happen with a waste of H^+ . It can be speculated from the O_2 -TPD curves and characterization results that the added Ni was most likely embedded in the g- C_3N_4 framework through coordination with N, preventing O_2 introduction for H^+ consuming. Therefore, H_2O_2 yielding of Ni-Pd@CN was higher than that of Fe-Pd@CN. Combined with all the merits of Fe and Ni, FeNi-Pd@CN could accumulate 1.69 mmol/L of H_2O_2 in 150 min. Through boost activity and selectivity, air could be used as the O_2 source instead of pure oxygen in other studies, which could cut down the cost for practical use.

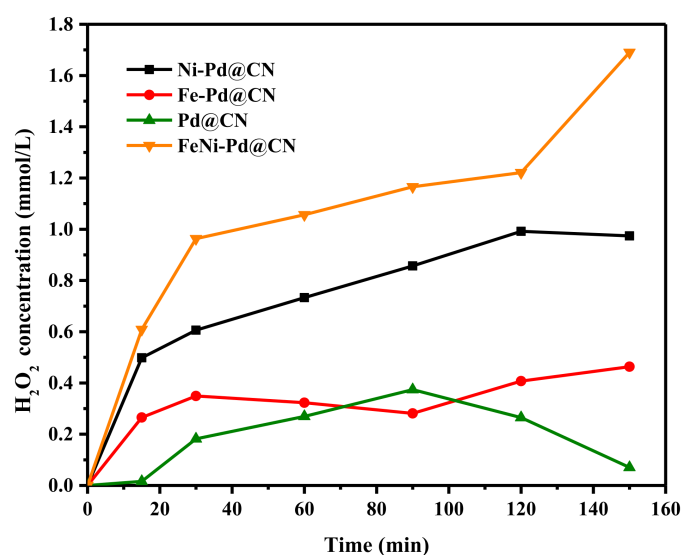
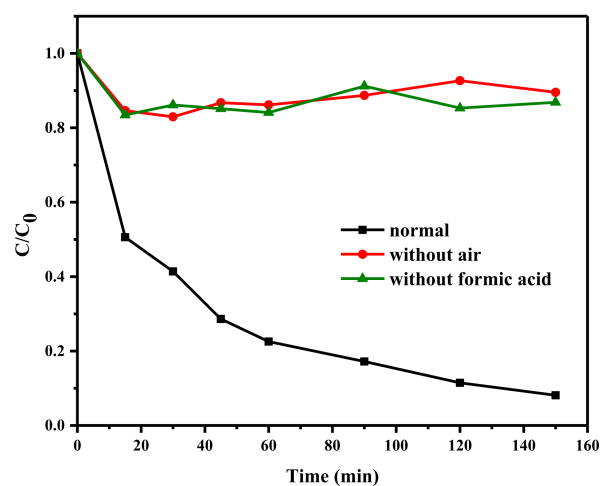


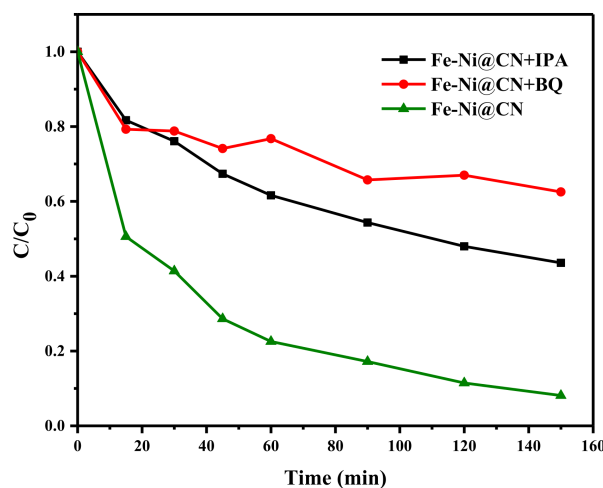
Figure 6. The H_2O_2 production ability over as-prepared catalysts (Catalyst dosage: 2 g/L; FA: 46.6 mmol/L; air; 200 mL/min).

3.5. Reaction Mechanism

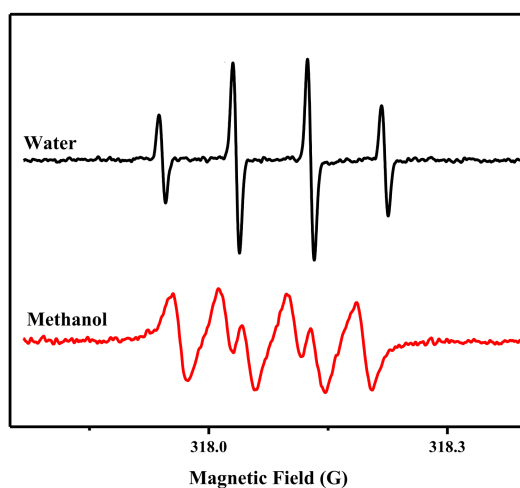
The reactions of organic removal begin with the FA decomposition and then O_2 reduction to H_2O_2 . Control experiments in Figure 7a confirmed the effect of FA and O_2 , and the results also suggested the removal of AR 73 in the FA/air/FeNi-Pd@CN system cannot be ascribed to adsorption. Once H_2O_2 was produced, Fenton reaction could happen due to the existence of Fe and Ni; thus, the system involves many reactive oxygen species (ROS), such as H_2O_2 , hydrogen superoxide radical ($\text{HO}_2\bullet$), and hydroxyl radical ($\bullet\text{OH}$) [37,38]. Scavengers including isopropanol (IPA, 3 M) and benzoquinone (BQ, 1 mM) are added in the reaction system to capture $\bullet\text{OH}$ and $\text{HO}_2\bullet$, respectively. The results in Figure 7b show that $\bullet\text{OH}$ and $\text{HO}_2\bullet$ have a strong inhibitory effect in varying proportions. ESR spin trapping experiments with dimethylpyridine N-oxide (DMPO), as the trapping agent also shows typical signals of DMPO- $\bullet\text{OH}$ and DMPO- $\bullet\text{O}_2^-$ in Figure 7c. $\text{HO}_2\bullet$ may participate in the Fe^{3+} reduction and is a crucial ROS in this system. The activity of Fe towards Fenton reaction is higher than Ni; thus, it is not surprising that the removal rate of AR 73 catalyzed by Fe-Pd@CN almost coincides with that of Ni-Pd@CN, despite the latter having more H_2O_2 in the system. Other experiments also pointed out that the presence of Ni could increase the $\bullet\text{OH}$ generation, probably facilitating the reduction in Fe^{3+} to Fe^{2+} [39].



(a)



(b)



(c)

Figure 7. (a) Degradation of FeNi-Pd@CN in different environments (AR 73 200 mg/L), (b) the H_2O_2 production ability over as-prepared catalysts, and (b) effect of IPA, BQ on the AR 73 degradation efficiency. (c) ESR DMPO- $\bullet\text{OH}$ and methanol- $\bullet\text{O}_2^-$ spectra of FeNi-Pd@CN catalyst (catalyst dosage: 2 g/L; FA: 46.6 mmol/L; air; 200 mL/min).

4. Conclusions

FeNi-Pd@CN catalyst was synthesized by thermal method, and its physical and chemical structures were fully characterized. In situ generation of H₂O₂ using formic acid and air was verified, and both •OH and HO₂• were generated during the reaction. Additionally, 92.0% of Acid Red 73 (200 mg/L) and 93.2% of tetracycline hydrochloride (10 mg/L) were removed in 150 min without any pH adjustment. Its high activity for organic removal was realized through: (i) the exposed Pd(111) facets with small size due to g-C₃N₄ support; (ii) the large accumulation of H₂O₂ due to Ni addition, and (iii) the high Fenton activity of Fe for ROS generation. The process only needs formic acid, catalysts, and air aeration, which is easy to realize in industrialization. It is worth studying further practical use in wastewater treatment.

Supplementary Materials: The following are available online at <https://www.mdpi.com/article/10.3390/app112210797/s1>, Figure S1: Nitrogen adsorption–desorption isotherms and pore size distribution curves, Figure S2: α-Fe₂O₃ (104) facet in the HRTEM image, Figure S3: Degradation of TC by different catalysts, Figure S4: XRD of fresh catalyst and after the fourth reused catalyst, Figure S5: The comparison of Pd 3d XPS spectra of different samples, Figure S6: O₂-TPD curves of different catalysts, Table S1: Elements contents of FeNi-Pd@CN calculated from the EDS results.

Author Contributions: Conceptualization, J.M. and L.W.; methodology, L.W.; validation, J.M.; formal analysis, L.W., Q.G. and J.S.; investigation, A.S.; resources, J.M. and L.L.; data curation, Q.G. and J.S.; writing—original draft preparation, L.W.; writing—review and editing, J.M.; visualization, L.W.; supervision, J.M.; project administration, L.L.; funding acquisition, J.M. and L.Z. All authors have read and agreed to the published version of the manuscript.

Funding: This research was funded by the National Natural Science Foundation of China (No.52000155), the Zhejiang Provincial Natural Science Foundation of China (No. LQ20E080002), the Public Benefits Projects of Ningbo (No. 202002N3055), and the Major Technological Innovation Projects of Ningbo National High-tech Zone (New Material Technology City, No.20201CX050018).

Institutional Review Board Statement: Not applicable.

Informed Consent Statement: Not applicable.

Data Availability Statement: The data presented in this study are available on request from the corresponding author.

Acknowledgments: The authors gratefully acknowledge the financial support from the National Natural Science Foundation of China, Zhejiang Provincial Natural Science Foundation of China, Ningbo Science and Technology Bureau, and the Science and Technology Innovation Bureau of Ningbo National High-tech Zone (New Material Technology City) as mentioned in the Funding Part. The authors also thank Shiyanjia Lab (www.shiyanjia.com (accessed on 28 March 2021)) for their participation in catalysts characterization.

Conflicts of Interest: The authors declare no conflict of interest.

References

1. Gagol, M.; Przyjazny, A.; Boczkaj, G. Wastewater treatment by means of advanced oxidation processes based on cavitation—A review. *Chem. Eng. J.* **2018**, *338*, 599–627. [[CrossRef](#)]
2. Collivignarelli, M.C.; Pedrazzani, R.; Sorlini, S.; Abbà, A.; Bertanza, G. H₂O₂ Based Oxidation Processes for the Treatment of Real High Strength Aqueous Wastes. *Sustainability* **2017**, *9*, 244. [[CrossRef](#)]
3. Pouran, S.R.; Aziz, A.A.; Daud, W.M.A.W. Review on the main advances in photo-Fenton oxidation system for recalcitrant wastewaters. *J. Ind. Eng. Chem.* **2015**, *21*, 53–69. [[CrossRef](#)]
4. Wang, N.; Zheng, T.; Zhang, G.; Wang, P. A review on Fenton-like processes for organic wastewater treatment. *J. Environ. Chem. Eng.* **2016**, *4*, 762–787. [[CrossRef](#)]
5. Liu, Q.; Yang, Y.; Lv, X.; Ding, Y.; Zhang, Y.; Jing, J.; Xu, C. One-step synthesis of uniform nanoparticles of porphyrin functionalized ceria with promising peroxidase mimetics for H₂O₂ and glucose colorimetric detection. *Sens. Actuators B Chem.* **2017**, *240*, 726–734. [[CrossRef](#)]
6. Zárte-Guzmán, A.I.; González-Gutiérrez, L.V.; Godínez, L.A.; Medel-Reyes, A.; Carrasco-Marín, F.; Romero-Cano, L.A. Towards understanding of heterogeneous Fenton reaction using carbon-Fe catalysts coupled to in-situ H₂O₂ electro-generation as clean technology for wastewater treatment. *Chemosphere* **2019**, *224*, 698–706. [[CrossRef](#)]

7. William, R.S. Cleaner industrial processes using hydrogen peroxide. *Pure Appl. Chem.* **2000**, *72*, 1289–1304.
8. Li, X.F.; Liu, W.P.; Ma, J.Q.; Wen, Y.Z.; Wu, Z.C. High catalytic activity of magnetic FeOx/NiOy/SBA-15: The role of Ni in the bimetallic oxides at the nanometer level. *Appl. Catal. B Environ.* **2015**, *179*, 239–248. [[CrossRef](#)]
9. Shaegh, S.A.M.; Nguyen, N.-T.; Ehteshami, S.M.M.; Chan, S.H. A membraneless hydrogen peroxide fuel cell using Prussian Blue as cathode material. *Energy Environ. Sci.* **2012**, *5*, 8225–8228. [[CrossRef](#)]
10. Samanta, C. Direct synthesis of hydrogen peroxide from hydrogen and oxygen: An overview of recent developments in the process. *Appl. Catal. A Gen.* **2008**, *350*, 133–149. [[CrossRef](#)]
11. Demirci, U.B.; Miele, P. Chemical hydrogen storage: ‘material’ gravimetric capacity versus ‘system’ gravimetric capacity. *Energy Environ. Sci.* **2011**, *4*, 3334–3341. [[CrossRef](#)]
12. Kopinke, F.-D.; Mackenzie, K.; Koehler, R.; Georgi, A. Alternative sources of hydrogen for hydrodechlorination of chlorinated organic compounds in water on Pd catalysts. *Appl. Catal. A Gen.* **2004**, *271*, 119–128. [[CrossRef](#)]
13. Yalfani, M.S.; Contreras, S.; Medina, F.; Sueiras, J. Direct generation of hydrogen peroxide from formic acid and O₂ using heterogeneous Pd/ γ -Al₂O₃ catalysts. *Chem. Commun.* **2008**, 3885–3887. [[CrossRef](#)]
14. Tan, N.; Yang, Z.; Gong, X.; Wang, Z.-R.; Fu, T.; Liu, Y. In situ generation of H₂O₂ using MWCNT-Al/O₂ system and possible application for glyphosate degradation. *Sci. Total Environ.* **2018**, *650*, 2567–2576. [[CrossRef](#)]
15. Thomas, A.; Fischer, A.; Goettmann, F.; Antonietti, M.; Müller, J.-O.; Schlögl, R.; Carlsson, J.M. Graphitic carbon nitride materials: Variation of structure and morphology and their use as metal-free catalysts. *J. Mater. Chem.* **2008**, *18*, 4893–4908. [[CrossRef](#)]
16. Ge, L.; Peng, Z.; Wang, W.; Tan, F.; Wang, X.; Su, B.; Qiao, X.; Wong, P.K. g-C₃N₄/MgO nanosheets: Light-independent, metal-poisoning-free catalysts for the activation of hydrogen peroxide to degrade organics. *J. Mater. Chem. A* **2018**, *6*, 16421–16429. [[CrossRef](#)]
17. Sun, B.-W.; Li, H.-J.; Yu, H.-Y.; Qian, D.-J.; Chen, M. In situ synthesis of polymetallic Co-doped g-C₃N₄ photocatalyst with increased defect sites and superior charge carrier properties. *Carbon* **2017**, *117*, 1–11. [[CrossRef](#)]
18. Ghosh, D.; Periyasamy, G.; Pandey, B.; Pati, S.K. Computational studies on magnetism and the optical properties of transition metal embedded graphitic carbon nitride sheets. *J. Mater. Chem. C* **2014**, *2*, 7943–7951. [[CrossRef](#)]
19. Jose, D.; Jagirdar, B.R. Synthesis and characterization of Pd(0), PdS, and Pd@PdO core-shell nanoparticles by solventless thermolysis of a Pd-thiolate cluster. *J. Solid State Chem.* **2010**, *183*, 2059–2067. [[CrossRef](#)]
20. Feng, Y.; Liao, C.; Kong, L.; Wu, D.; Liu, Y.; Lee, P.-H.; Shih, K. Facile synthesis of highly reactive and stable Fe-doped g-C₃N₄ composites for peroxymonosulfate activation: A novel nonradical oxidation process. *J. Hazard. Mater.* **2018**, *354*, 63–71. [[CrossRef](#)] [[PubMed](#)]
21. Niu, P.; Zhang, L.; Liu, G.; Cheng, H.-M. Graphene-Like Carbon Nitride Nanosheets for Improved Photocatalytic Activities. *Adv. Funct. Mater.* **2012**, *22*, 4763–4770. [[CrossRef](#)]
22. Ma, T.; Tang, Y.; Dai, S.; Qiao, S.Z. Proton-Functionalized Two-Dimensional Graphitic Carbon Nitride Nanosheet: An Excellent Metal-/Label-Free Biosensing Platform. *Small* **2014**, *10*, 2382–2389. [[CrossRef](#)] [[PubMed](#)]
23. Laokul, P.; Amornkitbamrung, V.; Seraphin, S.; Maensiri, S. Characterization and magnetic properties of nanocrystalline CuFe₂O₄, NiFe₂O₄, ZnFe₂O₄ powders prepared by the Aloe vera extract solution. *Curr. Appl. Phys.* **2011**, *11*, 101–108. [[CrossRef](#)]
24. Bertolini, J.C.; Delichere, P.; Khanra, B.C.; Massardier, J.; Noupa, C.; Tardy, B. Electronic properties of supported Pd aggregates in relation with their reactivity for 1,3-butadiene hydrogenation. *Catal. Lett.* **1990**, *6*, 215–223. [[CrossRef](#)]
25. Lei, W.; Portehault, D.; Dimova, R.; Antonietti, M. Boron Carbon Nitride Nanostructures from Salt Melts: Tunable Water-Soluble Phosphors. *J. Am. Chem. Soc.* **2011**, *133*, 7121–7127. [[CrossRef](#)]
26. Yu, H.; Shi, R.; Zhao, Y.; Bian, T.; Zhao, Y.; Zhou, C.; Waterhouse, G.I.N.; Wu, L.Z.; Tung, C.H.; Zhang, T. Alkali-Assisted Synthesis of Nitrogen Deficient Graphitic Carbon Nitride with Tunable Band Structures for Efficient Visible-Light-Driven Hydrogen Evolution. *Adv. Mater.* **2017**, *29*, 1605148. [[CrossRef](#)]
27. Ungureanu, A.; Dragoi, B.; Chiriac, A.; Ciotonea, C.; Royer, S.; Duprez, D.; Mamede, A.S.; Dumitriu, E. Composition-Dependent Morphostructural Properties of Ni-Cu Oxide Nanoparticles Confined within the Channels of Ordered Mesoporous SBA-15 Silica. *ACS Appl. Mater. Interfaces* **2013**, *5*, 3010–3025. [[CrossRef](#)]
28. Berríos, C.; Cardenas-Jiron, G.; Marco, J.; Gutiérrez, C.; Ureta-Zañartu, M.S. Theoretical and Spectroscopic Study of Nickel(II) Porphyrin Derivatives. *J. Phys. Chem. A* **2007**, *111*, 2706–2714. [[CrossRef](#)]
29. Mansour, A.N.; Melendres, C.A. Characterization of Slightly Hydrated Ni(OH)₂ by XPS. *Surf. Sci. Spectra* **1994**, *3*, 247–254. [[CrossRef](#)]
30. Yao, Y.; Chen, H.; Lian, C.; Wei, F.; Zhang, D.; Wu, G.; Chen, B.; Wang, S. Fe, Co, Ni nanocrystals encapsulated in nitrogen-doped carbon nanotubes as Fenton-like catalysts for organic pollutant removal. *J. Hazard. Mater.* **2016**, *314*, 129–139. [[CrossRef](#)] [[PubMed](#)]
31. Shi, Y.-C.; Feng, J.-J.; Lin, X.-X.; Zhang, L.; Yuan, J.; Zhang, Q.-L.; Wang, A.-J. One-step hydrothermal synthesis of three-dimensional nitrogen-doped reduced graphene oxide hydrogels anchored PtPd alloyed nanoparticles for ethylene glycol oxidation and hydrogen evolution reactions. *Electrochim. Acta* **2018**, *293*, 504–513. [[CrossRef](#)]
32. Hong, W.; Shang, C.; Wang, J.; Wang, E. Bimetallic PdPt nanowire networks with enhanced electrocatalytic activity for ethylene glycol and glycerol oxidation. *Energy Environ. Sci.* **2015**, *8*, 2910–2915. [[CrossRef](#)]
33. Qin, X.; Li, H.; Xie, S.; Li, K.; Jiang, T.-W.; Ma, X.-Y.; Jiang, K.; Zhang, Q.; Terasaki, O.; Wu, Z.; et al. Mechanistic Analysis-Guided Pd-Based Catalysts for Efficient Hydrogen Production from Formic Acid Dehydrogenation. *ACS Catal.* **2020**, *10*, 3921–3932. [[CrossRef](#)]

34. Jiang, B.; Zhang, X.-G.; Jiang, K.; Wu, D.-Y.; Cai, W.-B. Boosting Formate Production in Electrocatalytic CO₂ Reduction over Wide Potential Window on Pd Surfaces. *J. Am. Chem. Soc.* **2018**, *140*, 2880–2889. [[CrossRef](#)]
35. Tian, P.; Ouyang, L.; Xu, X.; Xu, J.; Han, Y.-F. Density functional theory study of direct synthesis of H₂O₂ from H₂ and O₂ on Pd(111), Pd(100), and Pd(110) surfaces. *Chin. J. Catal.* **2013**, *34*, 1002–1012. [[CrossRef](#)]
36. Bai, N.B. Evaluation of the energy of activation of chemisorption for H₂ and O₂ on transition d-metals. *J. Chem. Ind. Eng.* **1981**, *3*, 217–223.
37. Xu, Y.; Ge, F.; Xie, M.; Huang, S.; Qian, J.; Wang, H.; He, M.; Xu, H.; Li, H. Fabrication of magnetic BaFe₁₂O₁₉/Ag₃PO₄ composites with an in situ photo-Fenton-like reaction for enhancing reactive oxygen species under visible light irradiation. *Catal. Sci. Technol.* **2019**, *9*, 2563–2570. [[CrossRef](#)]
38. Li, C.; Wu, J.; Peng, W.; Fang, Z.; Liu, J. Peroxymonosulfate activation for efficient sulfamethoxazole degradation by Fe₃O₄/β-FeOOH nanocomposites: Coexistence of radical and non-radical reactions. *Chem. Eng. J.* **2019**, *356*, 904–914. [[CrossRef](#)]
39. de Souza, W.F.; Guimarães, I.R.; Oliveira, L.C.; Giroto, A.S.; Guerreiro, M.C.; Silva, C.L. Effect of Ni incorporation into goethite in the catalytic activity for the oxidation of nitrogen compounds in petroleum. *Appl. Catal. A Gen.* **2010**, *381*, 36–41. [[CrossRef](#)]